The Astrophysical Journal, 980:96 (9pp), 2025 February 10 https://doi.org/10.3847/1538-4357/adaa7c

Delay of Near-relativistic Electrons with Respect to Type III Radio Bursts throughout the Inner Heliosphere

J. G. Mitchell[1], E. R. Christian[1], G. A. de Nolfo[1], C. M. S. Cohen[2], M. E. Hill[3], A. Kouloumvakos[3], A. W. Labrador[2], R. A. Leske[2], D. J. McComas[4], R. L. McNutt, Jr.[3], D. G. Mitchell[3], M. Shen[4], N. A. Schwadron[5], M. E. Wiedenbeck[6], S. D. Bale[7,8], and M. Pulupa[8]
[1] NASA Goddard Space Flight Center, Greenbelt, MD 20771, USA; john.g.mitchell@nasa.gov
[2] California Institute of Technology, Pasadena, CA 91125, USA
[3] Johns Hopkins University, Applied Physics Laboratory, Laurel, MD 20723, USA
[4] Department of Astrophysical Sciences, Princeton University, Princeton, NJ 08544, USA
[5] University of New Hampshire, Durham, NH 03824, USA
[6] Jet Propulsion Laboratory, California Institute of Technology, Pasadena, CA 91109, USA
[7] Physics Department, University of California, Berkeley, CA 94720-7300, USA
[8] Space Sciences Laboratory, University of California, Berkeley, CA 94720-7450, USA
Received 2024 November 5; revised 2025 January 13; accepted 2025 January 13; published 2025 February 6

Abstract

Energetic electrons accelerated by solar eruptive events are frequently observed to have inferred injection times that appear significantly delayed with respect to electromagnetic emission including type III radio bursts. This is noteworthy because type III radio emission is produced by streaming suprathermal electrons, and thus this observed delay implies either a delayed injection/release of higher-energy electrons, compared with the suprathermal population, and/or a delay of the electrons observed in situ in transit through the interplanetary medium. A number of studies have investigated these delays with spacecraft located at 1 au. In this study, we examine energetic electron onsets and type III radio bursts observed by the Integrated Science Investigation of the Sun (IS⊙IS) and the FIELDS Radio Frequency Spectrometer instrument on Parker Solar Probe at a variety of heliocentric distances. With these observations, we can uniquely decouple the effects of acceleration and transport and shed light on the source of these delays. We present a survey of electron events observed by IS⊙IS within the first ∼6 yr of the mission, including their delays with respect to type III emission between ∼0.1 and 0.8 au. These results suggest that energetic electron delays with respect to type III radio bursts are not purely produced by a delayed injection/release as has been suggested, implying that transport processes play a role.

Unified Astronomy Thesaurus concepts: Solar energetic particles (1491); Interplanetary physics (827); Solar radio emission (1522)

1. Introduction

Solar energetic electrons are known to be accelerated in eruptive events including magnetic reconnection-driven solar flares and shocks driven by coronal mass ejections (CMEs; e.g., D. V. Reames 2013; N. Dresing et al. 2020). L. Wang et al. (2012) report that in situ measurements of energetic electrons are almost always directly associated with type III radio emission. Type III radio bursts are produced via a "bump-on-tail" plasma instability caused by streaming ∼2–25 keV electrons (G. A. Dulk et al. 1987; A. Buttighoffer 1998; H. A. S. Reid & H. Ratcliffe 2014). As these electrons stream out from the corona along open field lines into the interplanetary medium, they produce Langmuir waves at frequencies proportional to $\sqrt{n_e}$, where n_e is the local solar wind electron density (T. S. Bastian et al. 1998). The Langmuir waves produced by this instability then decay to produce type III radio emission. Thus, this emission is observed to rapidly drop from high frequencies (produced in regions of high electron density in the solar corona) to low frequencies (corresponding to the ambient solar wind density moving radially out from the Sun).

Despite the close correlation between in situ near-relativistic ($\gtrsim$50 keV) electron observations and type III radio bursts, it is unclear whether the near-relativistic electrons observed in situ and the type III–producing electrons are part of a single population (and injected at the same time) or whether they are injected at different stages of the solar eruptive event.[9] A number of studies have found characteristic delays of ∼10 minutes between the type III radio emission and the inferred injection of higher-energy (typically hundreds of keV) electrons (S. Krucker et al. 1999; D. K. Haggerty & E. C. Roelof 2002; A. Klassen et al. 2002; L. Wang et al. 2006; A. Kouloumvakos et al. 2015; I. C. Jebaraj et al. 2023). The observation of these delays led these researchers to conclude that the near-relativistic electrons observed in situ are injected later than the lower-energy electrons that excite the type III radio bursts. In contrast, H. V. Cane (2003) argued that the near-relativistic electrons are injected at the same time as the lower-energy electrons but are delayed in transit through the interplanetary medium.

[9] We note that we are using the term "injected" to match the historical studies on this topic. However, it is possible that in the scenario of scatter-free transport of electrons through the heliosphere that the low- and high-energy electrons were *injected* into the acceleration mechanism at the same time but the high-energy electrons were delayed through a later release from the acceleration site. Throughout this work, we use the term "injected" to indicate a delayed release from the Sun for any reason.

The observation of a subset of events in their sample that have no measurable delay between the near-relativistic electrons and the type III radio bursts led S. Krucker et al. (1999) to conclude that there are two classes of events: those in which the near-relativistic electrons and the type III–producing electrons are accelerated at the same time, and those in which the near-relativistic electrons are accelerated later than the type III–producing electrons. D. K. Haggerty & E. C. Roelof (2002) suggested that the near-relativistic electrons are accelerated by a CME-driven shock, attributing the observed delay to the time it takes for a CME-driven shock to propagate through the solar corona and accelerate electrons to near-relativistic energies. A. Klassen et al. (2002) reached a similar conclusion based on a comparison of four electron events with both type II and type III radio bursts. I. C. Jebaraj et al. (2023) performed a case study of an SEP event observed by Solar Orbiter <1 au that suggested that, in the acceleration of low-energy electrons, there is a mix of flare and shock acceleration mechanisms, while for the high-energy electrons, the acceleration and later release was mostly a shock-associated phenomenon in a highly structured corona.

H. V. Cane (2003) and H. V. Cane & W. C. Erickson (2003) compared the delays in near-relativistic electrons with the time it takes a type III radio burst to drift to the local plasma frequency. That study found a correlation (correlation coefficient 0.81) between the electron delay and the type III radio drift time as well as a weaker correlation (correlation coefficient of 0.66 for a subset of events with higher intensity) between the electron delay and the ambient solar wind density, implying that the near-relativistic and type III–producing electrons are part of a single population, both delayed in transit through the interplanetary medium. However, L. Wang et al. (2011) found that, while there is evidence for near-relativistic electron scattering near 1 au, the increased path length implied by this scattering cannot account for the typical delays observed. Thus, they conclude that the high-energy electrons are injected later than the lower-energy electrons that produce the type III emission.

The above studies used data from spacecraft located at 1 au. One goal of the Parker Solar Probe (N. J. Fox et al. 2016) mission is to shed light on these types of questions and disentangle the roles of acceleration and transport in the observed characteristics of solar energetic particle (SEP) enhancements. In this work, we examine the delay between energetic electrons and type III radio bursts using the Integrated Science Investigation of the Sun (IS⊙IS; D. J. McComas et al. 2016) and the Electromagnetic Fields Experiment (FIELDS; S. D. Bale et al. 2016) Radio Frequency Spectrometer (RFS; M. Pulupa et al. 2017) on Parker Solar Probe at a range of heliocentric distances to investigate the proposed sources of the delays observed in near-relativistic electrons with respect to type III radio bursts, in particular the overarching question of whether these delays can be attributed primarily to acceleration or transport. If, indeed, the observed delay in the near-relativistic electrons is purely produced by a delayed injection at the solar source, we would expect to observe this delay regardless of the heliocentric distance of the Parker Solar Probe spacecraft at which the event is measured (accounting for the propagation time of both the near-relativistic electrons and the type III emission). Thus, in the case of the delayed injection scenario, the distribution of delays is expected to be consistent regardless of observing distance from the Sun. Conversely, if the electrons are delayed in transport through the interplanetary medium, we would expect there to be a relationship between the observed distribution of delays and the distance of the observing spacecraft. In this work, we present electron delay characteristics with respect to type III radio emission from the first $\sim$6 yr of the Parker Solar Probe mission (spanning from launch in 2018 August to the most recent data at the time of writing from 2024 September) to investigate the source of these delays.

2. Instrumentation

The IS⊙IS instrument suite on Parker Solar Probe includes two Energetic Particle Instruments covering low energies (EPI-Lo; M. Hill et al. 2017) and high energies (EPI-Hi; M. E. Wiedenbeck et al. 2017), respectively. The EPI-Hi instrument measures energetic electrons from $\sim$0.5 to 8 MeV. The two sunward-pointing apertures in EPI-Hi, referred to as the High Energy Telescope (HET)-A and the Low Energy Telescope (LET)-A, were utilized for this work because they cover similar electron energy ranges but with slightly different pointing directions and energy-dependent geometry factors (M. E. Wiedenbeck et al. 2017).

EPI-Lo measures suprathermal and near-relativistic electrons in the range $\sim$70–300 keV. In this work, we utilize the EPI-Lo "ChanE" data from the sunward-pointing wedge (wedge 3). ChanE is the primary EPI-Lo channel used for electron measurements, though it can have significant contamination from high-energy ions when the foreground high-energy ion flux is sufficiently high (J. G. Mitchell et al. 2021). The detection efficiency of EPI-Lo for high-energy ions is roughly an order of magnitude lower than that of electrons at measured energies of $\lesssim$300 keV (J. G. Mitchell 2022; therefore, we used $<$100 keV measurements to minimize the risk of ion contamination in the ChanE data. From this point, we will refer to the ChanE data as electron data, as we have taken into account ion contamination and believe that this channel is dominated by foreground electron measurements during the considered intervals. The design of the EPI-Hi instruments minimizes the risk of ion contamination in the electron channels, and thus these considerations were not required when analyzing data from those instruments.

For this study, we also utilized the Parker Solar Probe FIELDS/RFS receiver (M. Pulupa et al. 2017). The low-frequency receiver (LFR) and high-frequency receiver (HFR) cover 10 kHz–1.7 MHz and 1.3 MHz–19.2 MHz bands, respectively. The RFS receivers operate on a 3.5 or 7 s cadence during solar encounters.

3. Data Selection

Energetic electron events were identified by surveying the 1 minute cadence $\sim$750 keV EPI-Hi HET and LET and $\sim$82 keV EPI-Lo electron count rate data. Prior to Spring of 2021, EPI-Hi did not provide electron data products with energy information at a $<$1 hr integration window outside of solar encounter periods (periods in which the spacecraft is located within 0.25 au of the Sun). Thus, for events identified before this change, the LET range 3 priority buffer data were utilized, as they are available at a 60 s cadence throughout the mission. Priority buffer data provides count rates with more limited information than the full science data at a cadence that ensures that important events are not missed due to telemetry

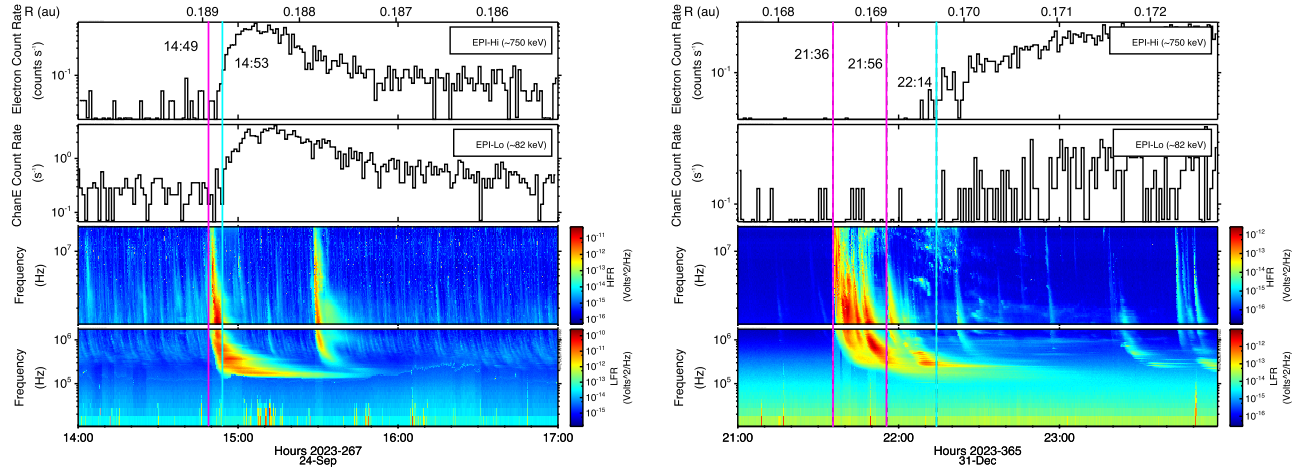

Figure 1. Examples of events that passed the described selection criteria (left; Event 22 in Table 1) and did not pass the selection criteria (right) within 0.2 au from the Sun. The text includes details as to why each event did or did not pass the selection criteria. Magenta vertical lines indicate the start of the type III radio burst in question (or intervals of continuous radio emission), and the cyan vertical line indicates the electron onset.

limitations (E. C. Stone et al. 1998). These data correspond to energetic electrons that stopped in range 3 of the LET instrument (the most shallow electron range of LET) across all energies. The distribution of energies over which electrons stop in range 3 is broad but peaks at ∼0.9 MeV (M. E. Wiedenbeck et al. 2017).

The survey yielded a list of 120 electron enhancements observed by EPI-Lo, EPI-Hi, or both sensors. These events were then filtered to only include those that were preceded by a clear type III radio burst <1 hr before the in situ electron onset and had a sufficiently high peak count rate above background ($\gtrsim 10\sigma$) and sufficiently fast initial rise time ($\gtrsim$1e-3 counts s^{-2}) to clearly identify the onset of the in situ energetic electrons. This also required events to have a sufficiently low pre-event background to not obscure the particle onset. Events were also discarded if they occurred during a type III radio storm (e.g., M. Pulupa et al. 2020), as the numerous, closely spaced type III radio bursts made it impossible to associate the energetic electron enhancement with a particular radio burst with any level of confidence. Exceptions were made when there was a single clearly dominant type III radio burst that reached the local plasma frequency during a type III storm. Events with onsets or radio data that may be obscured by a gap in data were also discarded. This filtering resulted in a list of 41 events observed by EPI-Hi and 34 events observed by EPI-Lo. Of these, 31 events were observed by both EPI-Hi and EPI-Lo, 10 were observed only by EPI-Hi with sufficient statistics to determine the onset time, and 3 were observed only by EPI-Lo with sufficient statistics to determine the onset time. The events observed only by EPI-Lo are likely dominated by the lowest energies, as expected for a steep power-law spectrum. Those observed only by EPI-Hi likely benefit from the significantly larger geometry factor of EPI-Hi (∼0.8 cm^2 sr at ∼2 MeV; M. E. Wiedenbeck et al. 2017) compared with a single EPI-Lo wedge (∼0.00616 cm^2 sr; J. G. Mitchell 2022).

Example events are shown in Figure 1. The event on 2023 September 24 (left) passed all selection criteria and was counted as a good event. While there is a type III radio storm happening during the event, there is only one type III radio burst that reaches the local plasma frequency, and thus we can uniquely match the in situ electrons with that radio burst. The electron signals in EPI-Hi and EPI-Lo are also sufficiently above background to be able to determine the onset easily. The event on 2023 December 31 (right) was not useful for this study, due to the multiple and complex type III radio emission observed for over 30 minutes leading up to the electron onset. Due to the need to associate each event with a single type III (or multiple bursts spaced closely in time), the uncertainty in the delay of this event meant that it was not a meaningful data point for our study. We note that this event appears to be correlated with a type II radio burst, and such bursts are frequently associated with the propagation of a CME-driven shock through the corona (e.g., H. V. Cane et al. 1987; E. W. Cliver et al. 1999). This, and similar events, may support a scenario in which the near-relativistic electron observed in situ are accelerated by an interplanetary shock. We also note that removing these types of event may introduce a bias against high-intensity but poorly connected events. The study of these types of events and their relationship to type II radio emission and connectivity will be the topic of a future study.

4. Analysis

The electron onset times were determined by calculating the time at which the signal rose to 2σ above the pre-event background, based on the electron count rate from the previous day, for three consecutive 1 minute time bins. Since EPI-Hi has multiple heads with similar energy ranges, but different boresight directions, onsets were recorded from both the HET and LET telescopes. The earliest onset was used as the representative time for an event, and the later onset was included in the uncertainty. After algorithmic determination of the onsets, these onset times were also checked by eye to ensure the obtained values were reasonable. When there was a clear enhancement before the onset detected by this procedure, that time was included in the uncertainty (there were no cases in which the onset appeared to be later than the algorithmically determined time). These cases were rare and usually resulted in only an additional 1 minute of uncertainty. The same method was applied to identification of the onset of the type III radio bursts. While events that took place during a type III radio storm were discarded, there were many events with multiple type III radio bursts preceding the in situ energetic electron onset. In these cases, the type III radio emission with the strongest power spectral density (PSD) was chosen as the most likely association; however, the earliest and latest reasonably

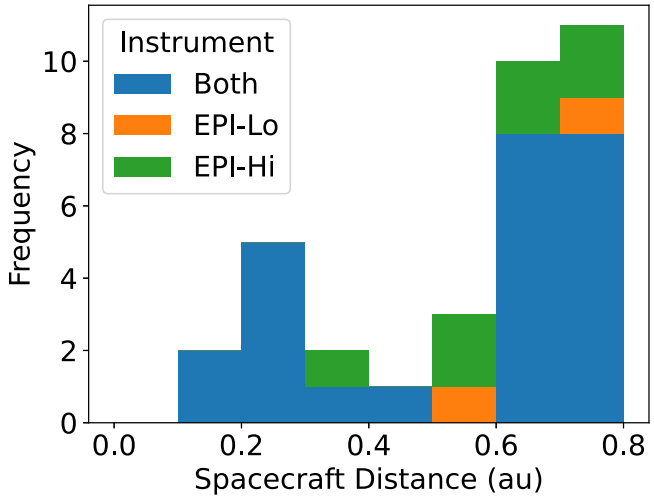

Figure 2. Distribution of Parker Solar Probe heliocentric distances at which the events in this study were observed. Stacked histogram colors correspond to events with significant enhancements observed by both EPI-Lo and EPI-Hi (blue), only EPI-Lo (orange), and only EPI-Hi (green).

associated type III radio burst times were included in the uncertainty. In many cases, the uncertainty in determining the type III radio burst associated with the in situ electron event was the most significant contributor of uncertainty. We also examined these events for the presence of in situ Langmuir waves, as the observation of these waves is indicative that the electron beam producing the type III emission is local to the spacecraft (e.g., H. A. S. Reid & E. P. Kontar 2017). The presence of in situ Langmuir waves associated with each event is indicated in Table 1.

The estimated solar release times of the near-relativistic electrons were then calculated using time-shifting analysis (TSA; e.g., V. Kolympiris et al. 2023) along a calculated Parker spiral with a solar wind speed measured by the Solar Probe ANalyzer for Ions (SPAN-I; R. Livi et al. 2022) instrument within the Solar Wind Electrons Alphas and Protons (SWEAP; J. C. Kasper et al. 2016) suite averaged over the first 2 hr of the event. In the two instances in which SPAN-I data were not available during the time period of interest, a baseline solar wind speed of 400 km s^{-1} was used. Travel times were calculated assuming electrons with energies of 760 keV in the case of EPI-Hi and 82 keV in the case of EPI-Lo. The 82 keV value for EPI-Lo corresponds to the center of the energy bin used for this study. The 760 keV value used for EPI-Hi is the average between the energy bins used for the EPI-Hi/HET and EPI-Hi/LET analysis. Measurements of energetic electrons by solid-state detectors often have significant contribution from higher-energy incident electrons in a particular energy bin, due to the increased scattering of electrons compared with ions (D. K. Haggerty & E. C. Roelof 2003; A. Labrador et al. 2023). Based on instrument Monte Carlo modeling, in both EPI-Lo and EPI-Hi, the largest contribution in a particular energy bin comes from incident electrons of that particular energy, with the second-largest contribution being from electrons with incident energies corresponding to the next-highest-energy bin (J. G. Mitchell 2022; A. Labrador et al. 2023). As the difference in electron travel time to the spacecraft between adjacent energy bins is consistently $\lesssim$60 s, this difference is within the uncertainty already produced by the 60 s integration time. Of course, there is likely a contribution from even higher-energy electrons in these bins, but assuming a typical falling power-law spectrum, this contribution is expected to be minimal. As well, for steep spectra, the representative energy of a particular bin will be lower than the center of the bin. Again, this uncertainty falls well within the intrinsic uncertainty produced by the 1 minute integration times. Another source of uncertainty in the TSA calculation is the Parker Spiral path length used to calculate the release time. This uncertainty was accounted for by calculating the electron travel time along a Parker Spiral path produced by a solar wind 50 km s^{-1} slower than the measured speed (resulting in a more curved spiral and therefore longer electron travel time) and the path length produced by solar wind 50 km s^{-1} faster than the measured speed (resulting in a less curved spiral and thus shorter electron travel time).

We investigated the use of velocity dispersion analysis (VDA; e.g., T. Laitinen et al. 2015) for this study; however, in particular at small heliocentric distances, the instruments do not have the required temporal resolution to show a dispersive onset for electrons of these energies. R. Vainio et al. (2013) compared the use of TSA and VDA in the case of solar energetic proton events and found that the inferred release time calculated by TSA was typically later than that calculated via VDA by an average of $\sim$10 minutes. In this study, we assumed scatter-free propagation along a Parker spiral, and thus the TSA method gives the latest possible release time.

Comparison with the injection time of the type III–producing electron population was accomplished by determining the onset of the type III emission at $\sim$2 MHz and correcting for the travel time of light along a straight path to the spacecraft location. This frequency was chosen because it is near the peak type III intensity (V. Krupar et al. 2014). Emission at these frequencies comes from $\sim 4R_S$, which may make a small difference calculated path length of the radio emission; however, this uncertainty is well within the 1 minute uncertainty contributed by the electron integration time. As previously mentioned, in many cases, the largest source of uncertainty came from the presence of multiple type III radio bursts closely spaced in time. Due to the large uncertainties determined in some events, we restricted the data set to only include events with a maximum uncertainty of 600 s, deeming any events with a greater values effectively meaningless for the purposes of this study. This reduced the total number of events observed by both sensors to 22, events observed only by EPI-Lo to 2, and events only observed by EPI-Hi to 9. A table with information on each event is provided in the Appendix.

The distribution of spacecraft heliocentric distances at which these events were measured is shown in Figure 2. The colors in the stacked histogram denote whether an event was observed by both EPI-Lo and EPI-Hi (blue), only EPI-Lo (orange), or only EPI-Hi (green). There is an obvious bias toward observing these events at distances $>$0.7 au, due to the highly eccentric orbit of the spacecraft, which limits the time during which the spacecraft is within 0.25 au during each orbit (approximately 10 days out of every $\sim$3 month orbit) (J. G. Mitchell et al. 2023). Due to the fairly limited number of events at small heliocentric distances, we plan to continue this study throughout the remainder of the mission in order to build up more statistics. However, with this study, we believe the statistics are sufficient to begin drawing conclusions.

We attempted to identify the solar source location of each event, and therefore, the longitudinal distance between the source region and the nominal spacecraft magnetic footpoint,

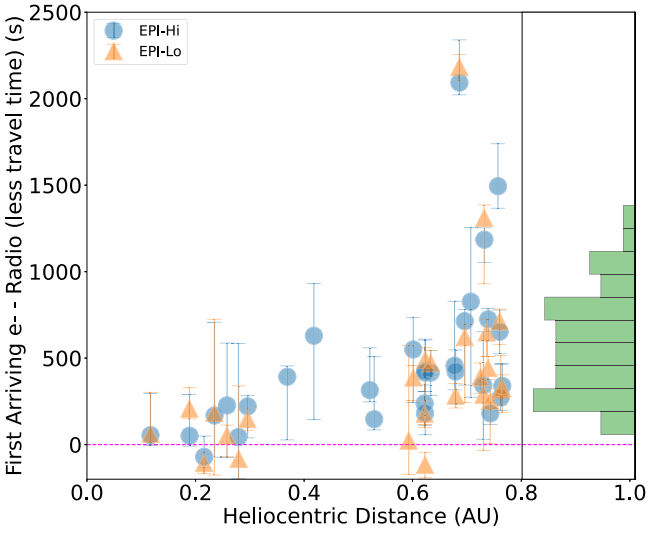

Figure 3. Estimated delay between an energetic electron injection and the start of a type III radio burst at the Sun observed by the IS⊙IS instruments on Parker Solar Probe as a function of heliocentric distance of the spacecraft. Representative data from spacecraft located at 1 au from H. V. Cane (2003) are shown as the green histogram on the same scale. Data points are shown as transparent, to allow the identification of overlapping points.

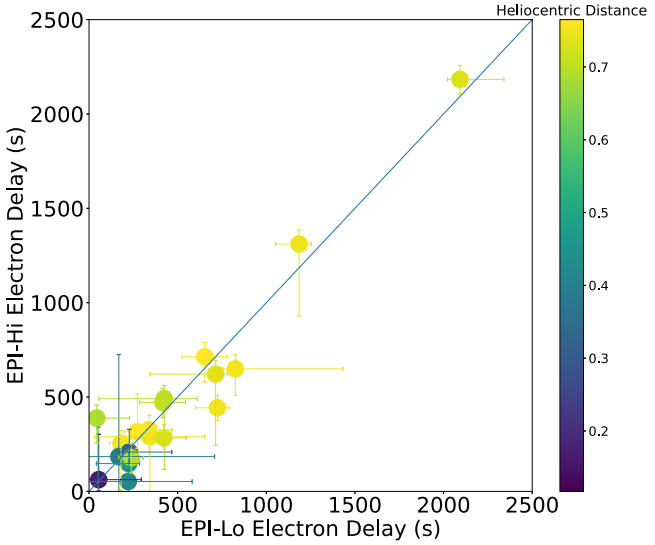

Figure 4. Scatter plot of the delay calculated from measurements of ∼82 keV electrons measured by EPI-Lo and ∼760 keV electrons measured by EPI-Hi. The color of each point indicates the heliocentric distance of the spacecraft when the event was measured.

calculated using a Parker Spiral with the locally measured solar wind speed at the time of event onset. S. Krucker et al. (1999), A. Kouloumvakos et al. (2015), and A. Posner et al. (2024) have suggested magnetic connectivity may play a role in the delays observed in energetic electrons, due to the need for those electrons to reach magnetic field lines connected to the observer. We utilized the NASA Community Coordinated Modeling Center (CCMC) Space Weather Database of Notifications, Knowledge, Information (DONKI[10]) to identify solar eruptive events with similar start times as the associated type III radio emission. We examined the catalog for solar flare and CME events with observed start times within ∼30 minutes of the type III radio burst in question. This was required because oftentimes events associated with CMEs are observed by coronagraphs later than the type III radio burst, due to the time it takes the CME to escape the corona. Once these events were identified, Solar Dynamics Observatory (SDO) Atmospheric Imaging Assembly (AIA; J. R. Lemen et al. 2012) images were searched to determine whether there was a different solar eruption (on the visible side of the Sun) than those identified in DONKI with timing that matched that of the type III radio emission more closely.

One of the event selection criteria used by D. K. Haggerty & E. C. Roelof (2003) was to restrict their study to only events with high anisotropy during the rise phase. The assumption was that these events were highly beamed and thus experienced minimal pitch angle scattering during propagation through the interplanetary medium and therefore could be considered "scatter-free." In order to examine the anisotropy of the events in this study, we utilized the weighted sum technique described in M. Brüdern et al. (2018), utilizing the two apertures of the EPI-Hi/HET telescope and the two wedges of EPI-Hi, both of which have large fields of view. The background was determined as the average count rate from the 20 minutes preceding the event onset. The first-order anisotropy was estimated for each background-subtracted time bin of the event onset and summed over the first 20 minutes of the event.

[10] https://kauai.ccmc.gsfc.nasa.gov/DONKI/

5. Results

A scatter plot showing the delay of the inferred electron injection time with respect to the inferred start of the type III emission is presented in Figure 3. The EPI-Lo data are shown as orange triangles and the EPI-Hi data are shown as blue circles, each with error bars encompassing the uncertainty produced by (1) multiple potential associated type III radio bursts, (2) uncertainty in Parker Spiral path length used for TSA, and (3) 60 s electron integration times. A histogram of the electron delays with respect to type III radio bursts observed at 1 au from H. V. Cane (2003) is shown on the right side to provide a direct comparison to the 1 au observations.

The delay in the events observed above background by both instruments in the IS⊙IS suite with sufficiently low uncertainty (i.e., less than 600 s) to be meaningful is shown in Figure 4. These are the same delays as shown in Figure 3. The color of each point indicates the heliocentric distance of the Parker Solar Probe spacecraft at which the event was observed. These events are clearly highly correlated and grouped along the 1:1 line (shown in blue) indicating a good agreement in the delay of a particular event between the ∼82 keV electrons measured by EPI-Lo and the ∼760 keV electrons measured by EPI-Hi. This indicates that the source of the delay appears to affect both the low- and high-energy electrons approximately similarly.

Figure 5 shows the same delays in the energetic electrons with respect to type III radio emission as shown in Figure 3 as a function of the difference in longitude between the spacecraft magnetic footpoint and the most likely solar source. Note that not all events shown in Figure 3 are shown in Figure 5, due to the inability to determine solar source regions for some events. Events with a negative (positive) value for the difference in longitude are those in which the solar source location is eastern (western) to the nominal spacecraft footpoint location.

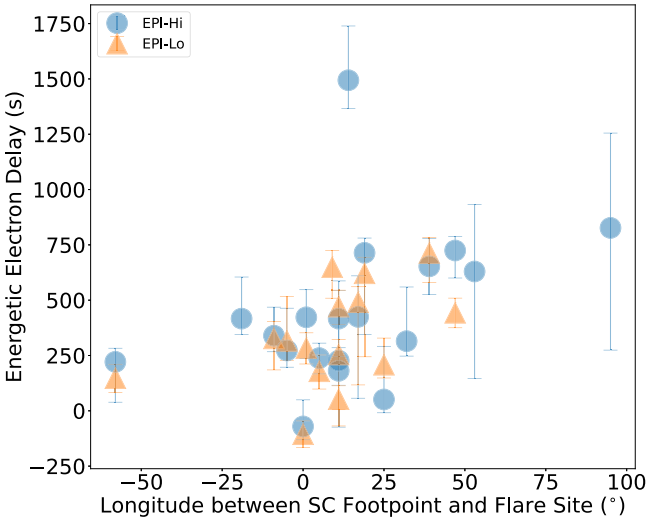

Figure 5. Delay of energetic electrons with respect to type III radio emission as a function of difference in longitude between the spacecraft magnetic footpoint and the likely solar source location. Negative (positive) values correspond to events in which the solar source was eastern (western) to the magnetic footpoint of the spacecraft.

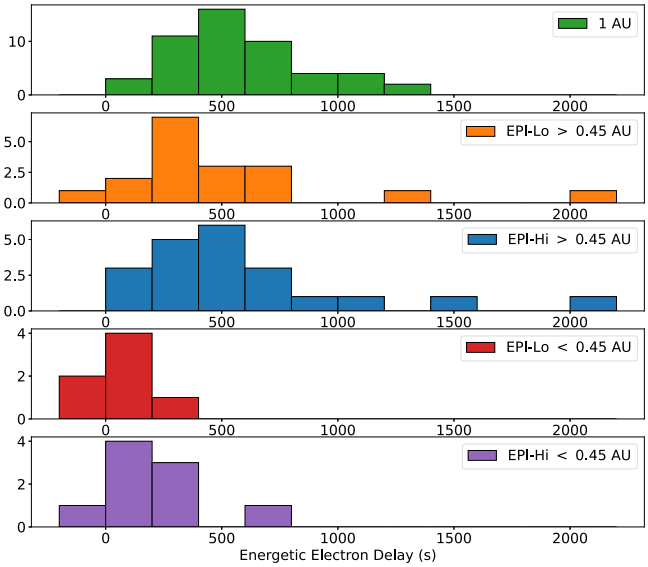

Figure 6. Distribution of energetic electron delays with respect to type III radio bursts from 1 au (green; from H. V. Cane 2003), EPI-Lo observations at distance >0.45 au (orange), EPI-Hi observations at distance >0.45 au (blue), EPI-Lo observations within 0.45 au (red), and EPI-Hi observations within 0.45 au (purple).

6. Discussion

If the delay between energetic electrons and type III radio bursts was purely due to a delayed injection of the energetic electrons, we would expect to see a relatively uniform distribution when accounting for the electron propagation time, presumably matching that observed at 1 au, regardless of the observing distance of the spacecraft. However, the observations in Figure 3 show an apparent relationship between the energetic electron delay with respect to type III radio bursts and the distance of the observer, in which longer delays are exclusively observed at farther distances. The distribution of delays as a function of heliocentric distance shown in Figure 3 appears to have a distribution in which it is possible to observe events with little or no delay at all distances, as noted in other studies. There are also several instances of points with negative delay times. All of those events, apart from one, have error bars that intercept the 0 line, and thus are consistent with 0 s delay. According to this analysis, the event of 2024 September 9 is consistent with a negative delay; however, the uncertainty brings the point close enough to the 0 s delay line that it is likely that one of the uncertainty factors was underestimated. We do not propose that, in this event, the high-energy electrons were injected *earlier* than the lower-energy electrons. Delays longer than ∼6 minutes (360 s), common at farther observing distances, are not observed at small heliocentric distances. Figure 6 shows the distribution of electron delays with respect to type III radio bursts at 1 au (green; from H. V. Cane 2003), EPI-Lo data observed from distances >0.45 au (orange), EPI-Hi data observed from distances >0.45 au (blue), EPI-Lo data observed within 0.45 au (red), and EPI-Hi data observed within 0.45 au (purple). The IS⊙IS data from distances >0.45 au are similar to the distribution at 1 au, while the distributions within 0.45 au exclusively have low calculated delays.

The relationship between near-relativistic electron delays with respect to type III radio bursts as a function of observing distance shown in Figures 3 and 6 indicates that transport effects likely play a role (perhaps exclusively) in the observed delays of energetic electrons. This likely indicates an effect that is dependent on the properties of the interplanetary medium through which the electrons are traveling. H. V. Cane (2003) found a potential correlation between the inferred delays of energetic electrons and the local solar wind plasma density at the location of the spacecraft. Similarly, A. Buttighoffer (1998) found that energetic electron beams were only observed by the HI-SCALE instrument (L. J. Lanzerotti et al. 1992) on Ulysses when the spacecraft was within "propagation channels" characterized primarily by low magnetic field fluctuations. Both factors could produce results in agreement with the findings of this work and will be the subjects of future investigations.

Similarly to the results of S. Krucker et al. (1999) (specifically those shown in the bottom of Figure 4 in that work), our results do not show any clear trend in the energetic electron delay with respect to type type III radio bursts as a function of longitudinal difference between the spacecraft magnetic footpoint and the likely solar source. There may be a slight trend in which, in general, events with greater separation between the spacecraft footpoint and the flare site have, on average, longer delays. It is possible that, with more events in the future, a relationship between the two values will become evident. Thus, the delays in this study cannot be explained purely by the time required for electrons to propagate onto magnetic field lines connected to the spacecraft. However, we cannot rule out at this may play a role in the observed delays, in particular as the nominal spacecraft footpoint used in this study was not backmapped to the source surface using an extrapolation such as the potential field source surface (e.g., P. Riley et al. 2006) model. In a statistical study analyzing ∼0.7–4 MeV electron events, I. G. Richardson et al. (2014) found a relationship between the longitude of a particular flare with respect to the STEREO spacecraft in which events closest to the spacecraft footpoint generally had shorter delays than those with greater longitudinal differences. The study by I. G. Richardson et al. (2014) included events with significantly larger angular differences between than the spacecraft footpoint and the flare site than what is included in the present study (note

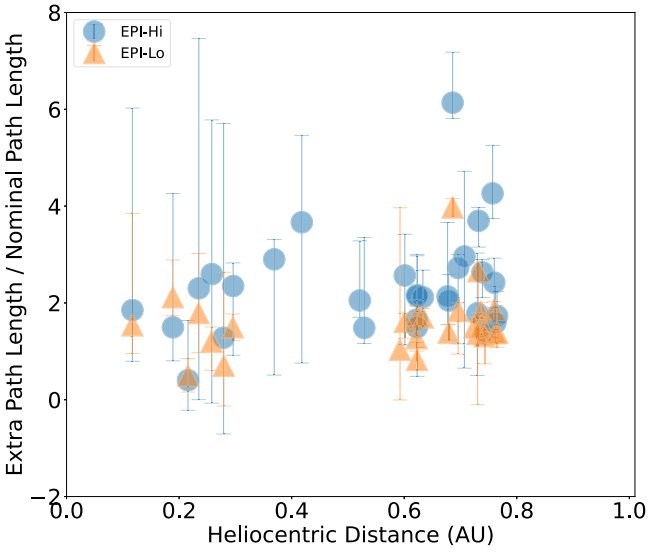

Figure 7. Inferred extra path length divided by the nominal path length as a function of heliocentric difference.

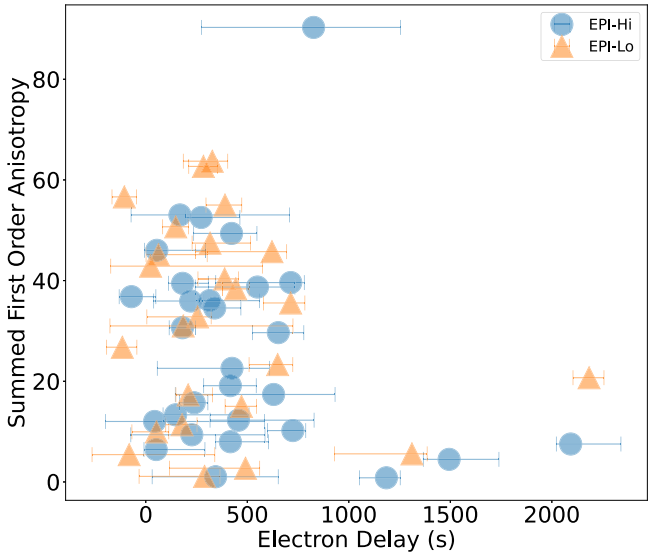

Figure 8. Estimates of first-order anisotropy as a function of near-relativistic electron delay with respect to type III radio bursts.

that the abscissa of the top right panel in Figure 15 of I. G. Richardson et al. (2014) extends from −180° to +180°, whereas in our study, Figure 5 only spans from −60° to 80°). Thus, if we begin to see more events with larger differences between the spacecraft footpoint and the flare site, we may begin to observe a similar relationship. A recent follow-up study by R. D. Strauss et al. (2023) simulated the onset delays examined by I. G. Richardson et al. (2014), taking into account interplanetary transport including particle scattering and cross-field (perpendicular) diffusion. The results of this work point toward a common accelerator for both electrons and protons and delays that are produced primarily by perpendicular diffusion.

To investigate the characteristics of the source of these delays, we calculated the ratio of the total path length of the electrons implied by the delay to the nominal path length. The results of this calculation are shown as a function of heliocentric distance in Figure 7. The distribution shows that the cause of these delays is fairly consistent as a function of heliocentric distance from the Sun and affects the electrons evenly as they stream through the interplanetary medium.

The absolute values of the estimates of the first-order anisotropy for each event are shown as a function of near-relativistic electron delay in Figure 8. In general, there is not an obvious relationship between the two values, apart from the fact that events with very long delays (i.e., >1000 s) all have a low first-order anisotropy. Events with delays between 0 and ∼800 s are observed with a range of first-order anisotropy estimates. This appears to indicate that there is not a strong relationship between near-relativistic electron anisotropy and delay with respect to type III radio bursts, apart from in fairly extreme cases of isotropy. This could also suggest that the longer path lengths traveled by the electrons are not produced solely by the effects of pitch-angle scattering—and may in fact be due to a field line that is longer itself due to wavy field lines or stretching of field lines due to transient interplanetary structures. We note that times in which the IS⊙IS instrument has poor pitch angle coverage could lead to systematically late apparent onsets, in particular in the case of highly anisotropic events. That said, in general, events that are observed to be highly anisotropic do not appear to have delays greater than ∼500 s.

7. Conclusions and Future Work

The results presented in this work indicate that the delays of energetic electrons with respect to type III radio bursts do not appear to be produced purely by a delayed injection into the acceleration mechanism or a delayed release from the solar source. With the relatively limited number of events at close distances we have accumulated so far in the mission, the near-relativistic electron delay with respect to type III radio bursts appears to be related to the distance at which the event is observed, with maximum delays increasing as a function of distance. We do not find any clear dependence on the electron delay with respect to type III radio bursts as a function of the longitudinal difference between the nominal spacecraft footpoint and the flare site, indicating that these delays are not purely produced by the time it takes near-relativistic electrons to diffuse across field lines to meet those connected to the spacecraft.

If we assume that the near-relativistic electron delay with respect to type III radio bursts is due, at least in part, to a transport effect as indicated by this work, the physical mechanisms that produce this highly variable delay remain uncertain. L. C. Tan et al. (2011) studied the anisotropy of electrons at a variety of energies and found that the scatter-free transport common to non-relativistic electrons appears to transition to diffusive transport at energies in the range of tens to hundreds of keV, governed primarily by the power spectral density of interplanetary magnetic field fluctuations. Above this transition energy, electrons are scattered by Alfvén waves producing an absence of scatter-free relativistic electron events. This is similar to the findings from A. Buttighoffer (1998) that electron beams were only observed when the Ulysses spacecraft was in "propagation channels." H. V. Cane (2003) found a weak correlation between energetic electron delays with respect to type III radio bursts and the local solar wind density, perhaps indicating that interactions between near-relativistic electrons and the ambient solar wind play a role in producing these delays.

Transport modeling studies have also demonstrated a radial dependence on the parallel mean free path, $\lambda_{||}$, of 85 keV electrons (R. D. T. Strauss et al. 2017) and 10 MeV protons (T. Laitinen et al. 2016) in which $\lambda_{||}$ is significantly larger close to the Sun. This effect, due to background turbulence, may help

explain the results of the present study. Additional modeling has demonstrated that $\lambda_{||}$ decreases with increasing electron energy (J. T. Lang et al. 2024), supporting the idea that near-relativistic electrons do not exhibit scatter-free transport to 1 au.

Even close to the Sun (i.e., $\lesssim$0.3 au), we observe some events with small delays between the type III radio emission and the calculated near-relativistic electron injection. A scenario in which shock acceleration plays a role in the delay is possible. However, it does not appear that a delayed injection can solely account for the delays observed at further distances from the Sun.

As the Parker Solar Probe mission progresses, we plan to continue collecting suitable electron events to further build up statistics, in particular at small heliocentric distances. It remains a possibility that we have simply not yet observed events with large delays close to the Sun and future events will support a delayed injection. We also plan to use further analysis of the radio, magnetic field, and solar wind data measured by the Parker Solar Probe instruments to shed light on the source of these delays if they are, indeed, produced by transport through the interplanetary medium. With Parker Solar Probe, we have the unique opportunity to conclusively determine whether this delay is produced by an acceleration effect, a transport effect, or a combination of the two.

Acknowledgments

We wish to acknowledge the support of NASA's Parker Solar Probe grant NNN06AA01C. We thank the Parker Solar Probe IS⊙IS, FIELDS, and SWEAP teams, including the engineers, technicians, administrators, and scientists, who developed the instruments used in this study. The IS⊙IS data and visualization tools are available to the community at https://spacephysics.princeton.edu/missions-instruments/isois; data are also available via the NASA Space Physics Data Facility (https://spdf.gsfc.nasa.gov/). The authors also wish to thank the reviewer for many thoughtful and insightful comments and suggestions that served to improve this work.

Appendix
Event List

Table 1 provides a complete list of near-relativistic electron events observed by the IS⊙IS instruments up to the time of writing. Information on each event includes the onset time for each IS⊙IS sensor and radio bursts, the distance of the Parker Solar Probe spacecraft at the time of the onset, and the calculated delay between the calculated release time of the near-relativistic electrons and that of the type III emitting suprathermal electrons.

Table 1
List Showing All Near-relativistic Electron Events Observed by IS⊙IS Sensors That Passed the Data Selection Requirements

Event Number	HET Onset (UTC)	LET Onset (UTC)	EPI-Lo Onset (UTC)	Radio Onset (UTC)	Distance (au)	EPI-Hi Delay (s)	EPI-Lo Delay (s)
1[a]	2020-May-27 18:11	2020-May-27 18:11	⋯	2020-May-27 18:04	0.37	398.02	⋯
2[a]	2021-Apr-17 16:32	2021-Apr-17 16:33	⋯	2021-Apr-17 16:21	0.42	633.04	⋯
3[a]	2021-May-28 23:38	2021-May-28 23:41	⋯	2021-May-28 23:02	0.69	2095.5	⋯
4	2021-Jun-09 12:09	2021-Jun-09 12:09	⋯	2021-Jun-09 12:03	0.76	279.7	329.09
5	2021-Jul-03 14:32	2021-Jul-03 14:32	2021-Jul-03 14:39	2021-Jul-03 14:28	0.74	164.2	225.02
6	2021-Oct-09 06:37	2021-Oct-09 06:36	2021-Oct-09 06:42	2021-Oct-09 06:29	0.77	339.14	326.81
7[a]	2021-Oct-28 15:34	2021-Oct-28 15:36	2021-Oct-28 15:40	2021-Oct-28 15:26	0.62	425.9	492.24
8[a]	2021-Nov-23 01:24	2021-Nov-23 01:24	2021-Nov-23 01:25	2021-Nov-23 01:23	0.12	54.45	63.00
9	2022-Mar-14 17:22	2022-Mar-14 17:23	⋯	2022-Mar-14 17:19	0.53	140.35	⋯
10[a]	2022-Jul-09 13:57	2022-Jul-09 13:48	2022-Jul-09 13:51	2022-Jul-09 13:33	0.74	825.22	649.44
11[a]	⋯	⋯	2023-Feb-24 13:06	2023-Feb-24 13:00	0.59	⋯	33.83
12 [a]	2023-Mar-13 03:17	2023-Mar-13 03:17	2023-Mar-13 03:19	2023-Mar-13 03:14	0.24	168.19	184.43
13	2023-May-16 11:30	2023-May-16 11:30	2023-May-16 11:39	2023-May-16 11:09	0.73	1186.42	1313.47
14	2023-May-16 17:28	2023-May-16 17:28	2023-May-16 17:29	2023-May-16 17:21	0.73	346.49	294.1
15[a]	2023-Jul-15 20:03	2023-Jul-15 20:05	⋯	2023-Jul-15 19:55	0.62	426.41	⋯
16	2023-Jul-24 18:05	2023-Jul-24 17:59	⋯	2023-Jul-24 17:44	0.71	831.46	⋯
17	2023-Aug-05 07:31	2023-Aug-05 07:28	⋯	2023-Aug-05 07:02	0.76	1480.74	⋯
18	2023-Aug-07 20:51	2023-Aug-07 20:51	2023-Aug-07 20:57	2023-Aug-07 20:39	0.76	640.11	690.64
19[a]	2023-Sep-21 12:49	2023-Sep-21 12:49	2023-Sep-21 12:50	2023-Sep-21 12:45	0.3	223.86	152.22
20	2023-Sep-22 17:18	2023-Sep-22 17:13	2023-Sep-22 17:12	2023-Sep-22 17:09	0.26	226.75	52.54
21	2023-Sep-24 14:51	2023-Sep-24 14:53	2023-Sep-24 14:55	2023-Sep-24 14:50	0.19	50.98	207.95
22[a]	2024-Jan-03 23:10	2024-Jan-03 23:08	2024-Jan-03 23:08	2024-Jan-03 23:07	0.28	44.96	−79.32
23	2024-Jan-27 05:34	2024-Jan-27 05:31		2024-Jan-27 05:22	0.68	476.73	⋯
24	2024-Mar-08 05:49	2024-Mar-08 05:51	2024-Mar-08 05:51	2024-Mar-08 05:39	0.6	549.48	387.48
25[a]	2024-May-20 05:25	2024-May-20 05:25	2024-May-20 05:26	2024-May-20 05:12	0.74	705.07	408.16
26[a]	⋯	⋯	2024-May-24 10:16	2024-May-24 10:02	0.73	⋯	418.84
27[a]	2024-Jun-26 02:12	2024-Jun-26 02:11	2024-Jun-26 02:12	2024-Jun-26 02:12	0.22	−70.59	−105.76
28	2024-Jul-16 13:44	2024-Jul-16 13:41	⋯	2024-Jul-16 13:35	0.52	320.9	⋯
29[a]	2024-Jul-24 17:20	2024-Jul-24 17:21	2024-Jul-24 17:26	2024-Jul-24 17:12	0.63	424.3	485.31
30	2024-Jul-29 12:55	2024-Jul-29 12:56	2024-Jul-29 13:00	2024-Jul-29 12:47	0.68	416.83	273.41
31[a]	2024-Jul-31 18:32	2024-Jul-31 18:32	2024-Jul-31 18:36	2024-Jul-31 18:19	0.7	713.58	620.78
32[a]	2024-Sep-06 14:04	2024-Sep-06 14:03	2024-Sep-06 14:07	2024-Sep-06 13:59	0.62	186.36	−106.78
33[a]	2024-Sep-06 15:26	2024-Sep-06 15:26	2024-Sep-06 15:30	2024-Sep-06 15:21	0.62	246.69	194.08

Note.
[a] Indicates that in situ Langmuir waves were observed in connection with this event.

ORCID iDs

J. G. Mitchell https://orcid.org/0000-0003-4501-5452
E. R. Christian https://orcid.org/0000-0003-2134-3937
G. A. de Nolfo https://orcid.org/0000-0002-3677-074X
C. M. S. Cohen https://orcid.org/0000-0002-0978-8127
M. E. Hill https://orcid.org/0000-0002-5674-4936
A. Kouloumvakos https://orcid.org/0000-0001-6589-4509
A. W. Labrador https://orcid.org/0000-0001-9178-5349
R. A. Leske https://orcid.org/0000-0002-0156-2414
D. J. McComas https://orcid.org/0000-0001-6160-1158
R. L. McNutt, Jr. https://orcid.org/0000-0002-4722-9166
D. G. Mitchell https://orcid.org/0000-0003-1960-2119
M. Shen https://orcid.org/0000-0002-3093-458X
N. A. Schwadron https://orcid.org/0000-0002-3737-9283
M. E. Wiedenbeck https://orcid.org/0000-0002-2825-3128
S. D. Bale https://orcid.org/0000-0002-1989-3596
M. Pulupa https://orcid.org/0000-0002-1573-7457

References

Bale, S. D., Goetz, K., Harvey, P. R., et al. 2016, SSRv, 204, 49
Bastian, T. S., Benz, A. O., & Gary, D. E. 1998, ARA&A, 36, 131
Brüdern, M., Dresing, N., Heber, B., et al. 2018, CEAB, 42, 2
Buttighoffer, A. 1998, A&A, 335, 295
Cane, H. V. 2003, ApJ, 598, 1403
Cane, H. V., & Erickson, W. C. 2003, JGRA, 108, 1203
Cane, H. V., Sheeley, N. R. J., & Howard, R. A. 1987, JGR, 92, 9869
Cliver, E. W., Webb, D. F., & Howard, R. A. 1999, SoPh, 187, 89
Dresing, N., Effenberger, F., Gómez-Herrero, R., et al. 2020, ApJ, 889, 143
Dulk, G. A., Goldman, M. V., Steinberg, J. L., & Hoang, S. 1987, A&A, 173, 366
Fox, N. J., Velli, M. C., Bale, S. D., et al. 2016, SSRv, 204, 7
Haggerty, D. K., & Roelof, E. C. 2002, ApJ, 579, 841
Haggerty, D. K., & Roelof, E. C. 2003, AdSpR, 32, 423
Hill, M., Mitchell, D., Andrews, G., et al. 2017, JGRA, 122, 1513
Jebaraj, I. C., Kouloumvakos, A., Dresing, N., et al. 2023, A&A, 675, A27
Kasper, J. C., Abiad, R., Austin, G., et al. 2016, SSRv, 204, 131
Klassen, A., Bothmer, V., Mann, G., et al. 2002, A&A, 385, 1078
Kolympiris, V., Papaioannou, A., Kouloumvakos, A., Daglis, I. A., & Anastasiadis, A. 2023, Univ, 9, 432
Kouloumvakos, A., Nindos, A., Valtonen, E., et al. 2015, A&A, 580, A80
Krucker, S., Larson, D. E., Lin, R. P., & Thompson, B. J. 1999, ApJ, 519, 864
Krupar, V., Maksimovic, M., Santolik, O., et al. 2014, SoPh, 289, 3121
Labrador, A., Mitchell, J. G., Christian, E., et al. 2023, ICRC (Nagoya), 38, 1315
Laitinen, T., Huttunen-Heikinmaa, K., Valtonen, E., & Dalla, S. 2015, ApJ, 806, 114
Laitinen, T., Kopp, A., Effenberger, F., Dalla, S., & Marsh, M. S. 2016, A&A, 591, A18
Lang, J. T., Strauss, R. D., Engelbrecht, N. E., et al. 2024, ApJ, 971, 105
Lanzerotti, L. J., Gold, R. E., Anderson, K. A., et al. 1992, A&AS, 92, 349
Lemen, J. R., Title, A. M., Akin, D. J., et al. 2012, SoPh, 275, 17
Livi, R., Larson, D. E., Kasper, J. C., et al. 2022, ApJ, 938, 138
McComas, D. J., Alexander, N., Angold, N., et al. 2016, SSRv, 204, 187
Mitchell, J. G. 2022, PhD thesis, George Washington Univ.
Mitchell, J. G., Cohen, C. M. S., Eddy, T. J., et al. 2023, ApJS, 264, 31
Mitchell, J. G., De Nolfo, G. A., Hill, M. E., et al. 2021, ApJ, 919, 119
Posner, A., Richardson, I. G., & Strauss, R. D. T. 2024, SoPh, 299, 126
Pulupa, M., Bale, S. D., Bonnell, J. W., et al. 2017, JGRA, 122, 2836
Pulupa, M., Bale, S. D., Badman, S. T., et al. 2020, ApJS, 246, 49
Reames, D. V. 2013, SSRv, 175, 53
Reid, H. A. S., & Kontar, E. P. 2017, A&A, 598, A44
Reid, H. A. S., & Ratcliffe, H. 2014, RAA, 14, 773
Richardson, I. G., von Rosenvinge, T. T., Cane, H. V., et al. 2014, SoPh, 289, 3059
Riley, P., Linker, J. A., Mikić, Z., et al. 2006, ApJ, 653, 1510
Stone, E. C., Cohen, C. M. S., Cook, W. R., et al. 1998, SSRv, 86, 357
Strauss, R. D., Dresing, N., Richardson, I. G., van den Berg, J. P., & Steyn, P. J. 2023, ApJ, 951, 2
Strauss, R. D. T., Dresing, N., & Engelbrecht, N. E. 2017, ApJ, 837, 43
Tan, L. C., Reames, D. V., Ng, C. K., Shao, X., & Wang, L. 2011, ApJ, 728, 133
Vainio, R., Valtonen, E., Heber, B., et al. 2013, JSWSC, 3, A12
Wang, L., Lin, R. P., & Krucker, S. 2011, ApJ, 727, 121
Wang, L., Lin, R. P., Krucker, S., & Gosling, J. T. 2006, GeoRL, 33, L03106
Wang, L., Lin, R. P., Krucker, S., & Mason, G. M. 2012, ApJ, 759, 69
Wiedenbeck, M. E., Angold, N. G., Birdwell, B., et al. 2017, ICRC (Busan), 301, 16